*Proceedings of the 21st ICSMGE, Vienna, Austria, 14 – 19 June 2026. Pistrol, Adam & Schweiger (eds.)*
*Published by: ÖGG, Austrian Society for Geomechanics, Salzburg, Austria, ISBN 978-3-9503898-4-5*
*https://doi.org/10.53243/ICSMGE2026-338*

# Dynamic Soil Arching in Column-Supported Embankments

**Piumali Abeywickrama,** K K W Premathilaka, D S Liyanapathirana, W Fuentes
*Western Sydney University, Sydney, NSW, Australia, Th.Kankanamge@westernsydney.edu.au*

ABSTRACT: Dynamic soil arching is an important phenomenon in column-supported embankments, profoundly shaping load transfer mechanisms and playing a crucial role in maintaining structural stability under cyclic loading. The focus of this paper is to investigate the soil arching in road embankments under repeated traffic loads, which are characterised by cyclic loading of variable intensities and frequencies. The paper begins with a literature review, summarising outcomes from recent in situ tests, laboratory experiments, and numerical simulations providing valuable insights into the mechanism of dynamic soil arching. The literature also reveals a persistent gap in the capacity of numerical models to accurately replicate the realistic soil behaviour under repeated cyclic loading. Most numerical studies to date have relied on constitutive models embedded within commercially available finite element programs. While these models may perform realistically in static analyses, they often fall short in capturing the soil behaviour under cyclic loading, particularly in saturated, fine-grained soils experiencing stiffness and strength degradation subsequently leading to fluidisation. The arching mechanism is fundamentally governed by the contrast in stiffness between the columns and the surrounding subsoil, a relationship that standard models are not typically equipped to represent with sufficient fidelity under cyclic loading conditions. This study addresses this limitation by conducting numerical simulations using a constitutive model based on bounding surface plasticity to capture the cyclic degradation of soft clay soils under embankments. The impact of traffic load intensity and frequency on the stability and efficiency of soil arching was investigated. The findings of this research show that the use of advanced constitutive models, such as those based on bounding surface plasticity, significantly improves the ability of numerical simulations to capture the complex cyclic behaviour of soft clay foundations and the evolution of dynamic soil arching.

KEYWORDS: Column-supported embankment, bounding surface plasticity, finite element method, dynamic arching.

## 1 INTRODUCTION

In column-supported embankments, load transfer from the embankment fill to columns and foundation soil is governed by the soil arching mechanism. The degree of soil arching is governed by the stiffness difference between the subsoil and columns. Under cyclic or dynamic loading, this beneficial arching effect does not remain constant but evolves in response to intensity of loading and degradation of subsoil. Trapdoor tests with Particle Image Velocimetry (PIV) have been used to demonstrate the formation and gradual weakening of soil arching in granular fills under repeated traffic loading (Bi et al. 2020). Large-scale physical model tests conducted by Niu et al. (2023) simulating high-speed train loads showed that arching effectiveness is frequency dependent and reach a maximum at about 25 Hz before diminishing with continued cycling. Combined physical and numerical studies have similarly reported that although arching initially develops under self-weight, it progressively adjusts under dynamic loading, with changes in stress concentration and load transfer mechanism (Ma et al. 2024). Trapdoor modelling has further demonstrated that fill density and subsoil stiffness govern both the magnitude and cyclic resilience of arching (Zhou et al. 2023). These findings highlight the need to examine not only the formation but also the evolution of soil arching under prolonged cyclic loading, particularly in systems with soft foundation soils and stiff columnar inclusions.

Numerical modelling has been used to systematically examine the effects of cyclic load amplitude, frequency, and material properties of foundation soil, columns and embankment fill on soil arching in column-supported embankments. Many early studies relied on the Mohr-Coulomb model available in commercially available software (e.g., ABAQUS or PLAXIS) to represent both the embankment fill and soft clay subsoil (Lang et al. 2023) and investigated long-term performance of embankments due to train-induced cyclic loading (Zhuang & Wang 2018). Also, Modified Cam Clay (MCC) model has been used to simulate the subsoil (soft clay) behaviour in studies involving high-speed railway loads (Han et al. 2015; Bian et al. 2024). To address the limitations in conventional soil constitutive models, several studies adopted advanced constitutive formulations to simulate the embankment fill behaviour in column-supported embankments. Pham & Dias (2019) used Hypoplasticity, capable of simulating the strain accumulation and small-strain stiffness degradation in ABAQUS via a user defined subroutine (UMAT) to model embankment fill under cyclic loading. However, the soft clay subsoil beneath the columns was still represented using the built-in Mohr–Coulomb model, which cannot capture cyclic degradation, anisotropy, irreversible strain accumulation or fluidization of the saturated subsoil.

While recent studies have advanced the simulation of embankment behaviour under cyclic loading, reliance on simple constitutive models for the foundation clay limits the ability to predict arching evolution. Models such as Mohr–Coulomb and Modified Cam Clay (MCC) are computationally efficient and adequate for the simulation of soil behaviour under monotonic loading, but they are not designed to replicate soil behaviour under cyclic loading conditions. They cannot capture stiffness and strength degradation, cyclic mobility, and stress reversal effects. This represents a significant research gap for column-supported embankments subjected to repeated heavy vehicle or train loading, particularly in understanding and predicting dynamic arching behaviour. To address this, a three-dimensional finite element model of a DCM-supported embankment was developed in this study, employing the constitutive model SANICLAY-B (Seidalinov & Taiebat 2014) to replicate the soft clay subsoil. The SANICLAY family of models, developed within the critical state framework, incorporates rotational hardening to account for anisotropy and, SANICLAY-B version, combines anisotropic hardening with a bounding surface plasticity, enabling realistic simulation of cyclic degradation, hysteresis, and progressive strain accumulation in soft clays. The predictive capability of the proposed approach was evaluated against the built-in Modified Cam Clay (MCC) model in ABAQUS/Standard (Dassault Systèmes, 2023), first at the element level and then within a soft clay layer of a finite-element model of a DCM-supported embankment. Finally, the SANICLAY-B model was used for the soft clay in a parametric study to quantify the influence of

cyclic-loading frequency and amplitude on the arching mechanism.

## 2 FINITE ELEMENT MODEL DEVELOPMENT FOR THE CASE STUDY

In the literature, there are no case studies available for embankments subjected to cyclic loading conditions with soil properties required to develop a finite element model. Hence, in this paper, the embankment geometry and subsoil stratigraphy were adopted from the Bangbo highway embankment project in Thailand, as detailed by Jamsawang et al. (2016), to verify the finite element model developed in ABAQUS/Standard (Dassault Systèmes, 2023).

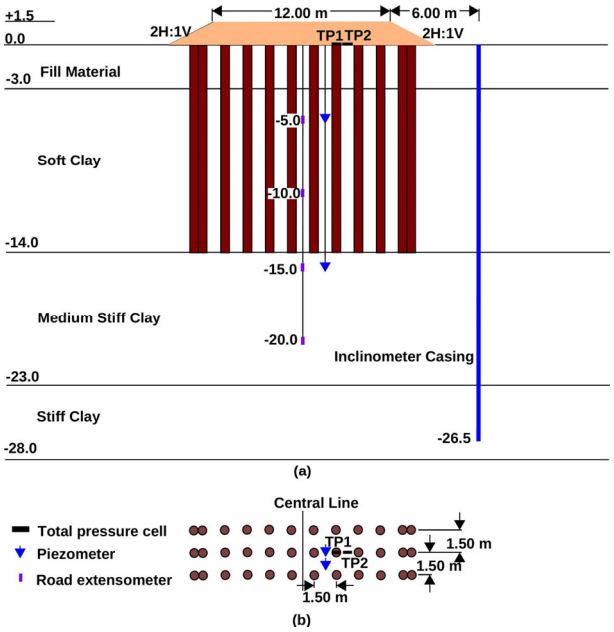


Figure 1. (a) Cross section and (b) Plan view of Bangbo Embankment in Thailand (Jamsawang et al. 2016)

The verification was conducted considering static loading as outlined by Jamsawang et al. (2016). The embankment is 1.5 m high with a 12 m-wide crest and 1(V):2(H) side slopes, founded on ground improved with Deep Cement Mixing (DCM) columns installed in a square grid at 1.5 m spacing. Each column is 0.6 m in diameter and 14 m long, with tips bearing on the medium stiff clay layer, and an additional tangential column was placed at the toe to enhance lateral resistance as shown in Figure 1. The three-dimensional finite element model was developed in ABAQUS/Standard (Dassault Systèmes, 2023) considering the symmetry of the problem. Only half of the embankment was modelled extending to a depth of 28 m (down to a rigid, impermeable layer). The horizontal length of the finite element model was extended 60 m to minimise boundary effects. A symmetrical boundary condition was applied along the center plane (x = 0), and the vertical faces at y = 0 and y = 1.5 m. The far field vertical boundary on the right-hand side of the slice (x = 60m) was restrained against horizontal movements (Ux = 0) while allowing tangential and vertical movements. The base was pinned restraining all translational degrees of freedom (Ux = Uy = Uz = 0). The groundwater table prescribed at 1.5 m below the ground surface to define the initial hydrostatic field. The subsurface profile comprises a 3 m-thick fill layer, underlain by 11 m of soft Bangkok clay, 9 m of medium stiff clay, and 5 m of stiff clay. The mesh employed 8-node brick elements with trilinear displacement and trilinear pore pressure interpolation for the subsoil and DCM columns, and 8-node linear brick elements for the embankment fill. The 3D finite element mesh developed in this study is shown in Figure 2.

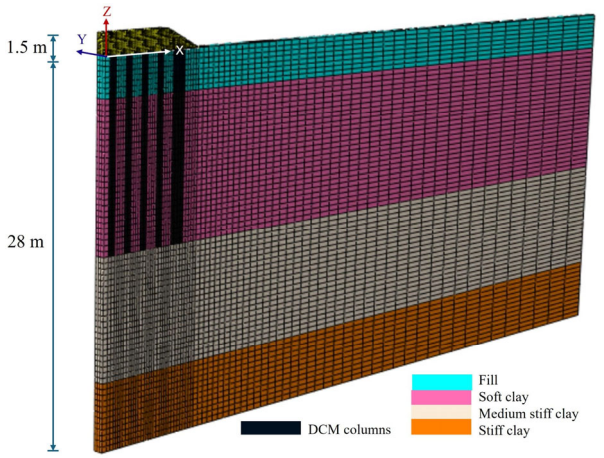


Figure 2. 3D finite element mesh

### 2.1 *Constitutive behaviour of soil and columns*

The embankment fill, medium stiff clay, stiff clay and DCM columns were modelled using the Mohr Coulomb model in ABAQUS/Standard (Dassault Systèmes, 2023). The material properties used in this study $\gamma, E, \nu, c, \emptyset,$ and $k$ represent unit weight, elastic modulus, poisson's ratio, cohesion, friction angle, and permeability coefficient, respectively. These values were adopted from Jamsawang et al. (2016) and are presented in Table 1.

Table 1. Parameters used for Mohr Coulomb model.

| Material | $\gamma$ (kN/m$^3$) | $E$ (MPa) | $\nu$ (-) | $c$ (kPa) | $\emptyset$ ($^0$) | $k$ (m/d) |
|---|---|---|---|---|---|---|
| Embankment | 20 | 20 | 0.33 | 10 | 30 | - |
| Fill material | 20 | 30 | 0.33 | 1 | 32 | $5 \times 10^{-1}$ |
| DCM column | 15 | 80 | 0.33 | 450* | 0 | $5 \times 10^{-4}$ |
| Medium stiff clay | 16 | 20 | 0.15 | 10 | 25 | $2.5 \times 10^{-4}$ |
| Stiff clay | 20 | 50 | 0.20 | 18 | 25 | $2.5 \times 10^{-4}$ |

*Undrained shear strength

The soft clay layer was modelled using SANICLAY-B. Seidalinov & Taiebat (2014) developed the SANICLAY-B model as a bounding-surface extension of the SANICLAY-D developed by Taiebat et al. (2010) within the critical state framework (Roscoe & Burland 1970). The capability of the model to capture cyclic effects was assessed against the built-in MCC formulation in ABAQUS/Standard (Dassault Systèmes, 2023) applied to the soft-clay layer. SANICLAY-B combines isotropic and rotational hardening with a bounding surface plasticity mechanism to realistically capture volumetric changes, stress-induced anisotropy, stiffness degradation, strain accumulation, and hysteresis under cyclic loading. Unlike conventional Mohr–Coulomb and MCC models, which rely on a fixed yield surface, SANICLAY-B allows plastic strains to develop within the traditionally elastic zone via a radial mapping rule with a moving projection center. Anisotropic hardening is introduced through the rotation of the bounding and plastic potential surfaces, while a damage-based hardening function accounts for progressive stiffness loss during stress reversals. The bounding surface ($F$) and plastic potential surface ($g$) are defined by Equations (1) and (2), respectively.

$$F = \frac{3}{2}(\bar{s} - \bar{p}\alpha):(\bar{s} - \bar{p}\alpha) - (N^2 - \frac{3}{2}\alpha:\alpha)\bar{p}(p_0 - \bar{p}) = 0 \quad (1)$$

$$g = \frac{3}{2}(\bar{s} - \bar{p}\alpha):(\bar{s} - \bar{p}\alpha) - (M^2 - \frac{3}{2}\alpha:\alpha)\bar{p}(p_\alpha - \bar{p}) = 0 \quad (2)$$

where

$$\bar{p} = p_c + b(p - p_c) \quad (3)$$

$$\bar{s} = s_c + b(s - s_c) \quad (4)$$

$p$ is the mean effective stress and $\boldsymbol{s}$ is the deviatoric tensor, defined by $\boldsymbol{s} = \sigma - pI$ where σ and $I$ denotes stress and identity tensor respectively. $\alpha$ is an internal variable based on the stress ratio tensor, $p_0$ and $p_\alpha$ are the size of the yield surface and plastic potential surface respectively. $N$ is a constant similar to critical stress ratio $M$. $\bar{p}$ and $\bar{s}$ denotes the hydrostatic and deviatoric components of image stress ($\bar{\sigma}$) on the bounding surface. $p_c$ and $s_c$ denotes the hydrostatic and deviatoric components of projection center ($\sigma_c$). $b$ is the similarity ratio that should be calculated as recommended by Seidalinov & Taiebat (2014).

The plastic modulus $K_P$ of SANICLAY-B is given by;

$$K_P = \bar{K}_P + \frac{hp_0^3}{\langle b|(b-1) - s\rangle} \quad (5)$$

where $s$ governs the size of the elastic nucleus and $\bar{K}_P$ is given by;

$$\bar{K}_P = -(\frac{\partial F}{\partial p_0}\bar{p}_{0+}\frac{\partial F}{\partial \alpha}\bar{\alpha}) \quad (6)$$

To replicate the continuous evolution of stress–strain loops and the associated stiffness degradation observed in experiments, the shape hardening parameter $h$ which governs the plastic modulus $K_P$, is expressed as a decaying function of plastic deviatoric strain, given by;

$$h = \frac{h_0}{1 + d} \quad (7)$$

where $h_0$ defines the initial shape hardening and influences the plastic modulus within the bounding surface and the rate of change of damage parameter $d$ is given by,

$$\dot{d} = a_d|\dot{\varepsilon}_q^p| \quad (8)$$

Higher values of $h_0$ reduce plastic strain accumulation and produce narrower stress–strain loops, indicating a stiffer response. The parameter $a_d$ governs the evolution of $d$, which progressively reduces $h$ and thus the plastic modulus, enabling simulation of stiffness loss under repeated loading. Seidalinov & Taiebat (2014) validated SANICLAY-B constitutive model against undrained cyclic triaxial tests on various clays and demonstrated that SANICLAY-B reproduces modulus reduction, damping evolution, stress–strain hysteresis, and permanent strain accumulation more accurately than earlier SANICLAY versions without a bounding-surface mechanism. To investigate dynamic soil arching, the SANICLAY-B model was implemented in ABAQUS/Standard (Dassault Systèmes, 2023) via a user-defined material subroutine (UMAT) coded in Fortran 90 (ISO/IEC, 1991) using Visual Studio 2022. The source code was first compiled and verified at the material-point level using the Incremental Driver (Niemunis, 2022) before integration into ABAQUS/Standard (Dassault Systèmes, 2023). Verification of the numerical implementation was achieved through reproduction of multiple undrained cyclic triaxial tests. The MCC parameters ($\kappa, \nu, \lambda, M_c$) and the additional SANICLAY-B parameters for Georgia Kaolin Clay (GKC) and Bangkok Clay are presented in Table 2. Both the enhanced cyclic capabilities of SANICLAY-B relative to conventional MCC and the correctness of the implementation in ABAQUS/Standard (Dassault Systèmes, 2023) are demonstrated by simulating the undrained cyclic triaxial response of Georgia Kaolin Clay (GKC). The GKC material parameters and testing protocol were adopted from Seidalinov, (2018).

SANICLAY-B material properties for Bangkok clay was calibrated based on the procedure recommended by Seidalinov (2018). The calibration procedure involves 10 primary model constants in addition to the necessary initial internal variables. The parameters λ, κ, and ν were adopted from Jamsawang et al. (2016), while the critical state stress ratio in triaxial compression $M_c$ was derived from Equation (9).

$$M = \frac{6\sin\phi}{3 - \sin\phi} \quad (9)$$

The critical state stress ratio in extension $M_e$ is assumed equal to $M_c$. The bounding surface parameter $N$ was set equal to $M$. The rotational hardening response was governed by parameters $C$ and $X$, with $X$ computed using the closed-form relation proposed by Dafalias et al. (2006).

$$\frac{\eta_k}{X} = \frac{B\varepsilon{\eta_k}^3 + {\eta_k}^2 + \left[2\left(1 - \left(\frac{\kappa}{\lambda}\right)\right) - BM_c^2\right]\varepsilon\eta_k - M_c^2}{2\varepsilon\left(1 - \left(\frac{\kappa}{\lambda}\right)\right)} \quad (10)$$

$$B = -\frac{2(1+\upsilon)\kappa}{9(1-2\upsilon)\lambda} \quad (11)$$

$$\eta_k = \frac{3(1 - K_0)}{(1 + 2K_0)} \quad (12)$$

where $K_0$ is the lateral earth pressure coefficient at rest. For $K_0$ loading paths, the coefficient $\varepsilon$ was set to 3/2, and the resulting value of $X$ was required to exceed unity. The parameter $C$, which controls the rate of rotation and distortion of the yield and plastic potential surfaces, was calibrated through trial simulations. In addition to the Modified Cam Clay (MCC) model, the SANICLAY-B model introduced rotational hardening to account for inherent and induced anisotropy through distinct yield and plastic potential surfaces. The SANICLAY-B formulation further integrates a bounding surface to more effectively capture cyclic response of clay soils under plastic deformations. These enhancements enable a more realistic simulation of cyclic and anisotropic soil response observed during experiments. Setting $C$=0 makes the model equivalent to MCC, which has an isotropic yielding. As embankment loading often induces directional soil behaviour, activation of a degree of anisotropy was considered advantageous for the present analysis. For dynamic analysis, the cyclic behaviour is activated through $h_0$ and $a_d$ by assigning nominal values of $h_0$=50 and $a_d$=1, because cyclic triaxial data are not available for the soil at the site to calibrate them. In general, $h_0$ and $a_d$ are calibrated through trial-and-error simulations against cyclic element test data, such as undrained cyclic triaxial or cyclic direct simple shear tests. The early-cycle hysteresis response is typically used to adjust $h_0$,

while the progressive strain accumulation and stiffness degradation over multiple cycles are used to refine $a_d$.

Table 2. Parameters used for SANICLAY-B.

| Category | Designation | Bangkok Clay | Georgia Kaolin Clay |
|---|---|---|---|
| Elasticity | $\kappa, \nu$ | 0.16, 0.15 | 0.037, 0.2 |
| Critical state | $\lambda, Mc, Me$ | 0.79, 0.89, 0.89 | 0.121, 0.87, 0.86 |
| Bounding surface | $N, h_0, ad$ | 0.89, 50, 1 | 0.8, 50, 7 |
| Rotational hardening | $C, X$ | 10, 1.7 | 3, 1.69 |
| Permeability (m/d) | $k$ | 5×10-4 | 1×10-4 |

Figure 3 shows the experimental undrained cyclic triaxial response. With increasing load cycles, small-strain tangential stiffness reduces, widening the stress-strain loops. This behaviour indicates plastic strain accumulation. The simulation by Seidalinov (2018) using SANICLAY-B reproduces these signatures of loop curvature: increasing loop area (energy dissipation), and mean-strain drift that captures the observed degradation. The close agreement between the simulation by this study and those reported by Seidalinov (2018) corroborates the accuracy of the implementation of the model in ABAQUS/Standard (Dassault Systèmes, 2023). By contrast, the ABAQUS/Standard (Dassault Systèmes, 2023) built-in MCC model yields comparatively narrow loops that are over-stiff near the origin and exhibit limited strain accumulation, thereby underestimating cyclic degradation and dissipation.

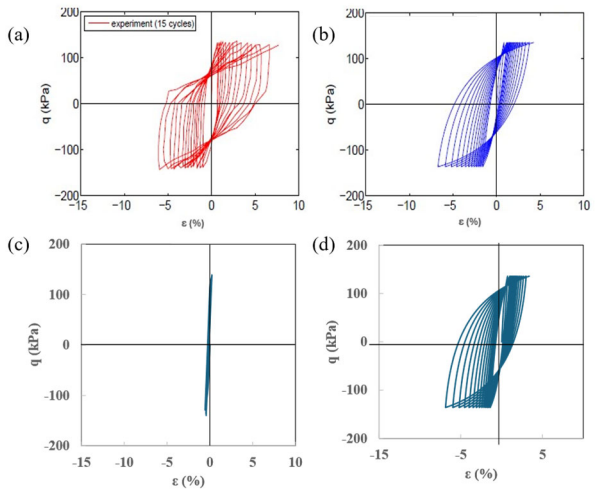


Figure 3. Cyclic stress–strain response at cyclic amplitude $q$=136 kPa over 15 cycles on GKC: (a) experiment data reported by Seidalinov, (2018); (b) simulation by Seidalinov, (2018) using SANICLAY-B; (c) simulation with MCC (d) simulation using SANICLAY-B implemented in ABAQUS/Standard (Dassault Systèmes, 2023)

## 2.2 *Validation of the 3D finite element model*

The staged construction of the embankment consists of four lifts of 0.5 m, 0.3 m, 0.4 m, and 0.3 m that were constructed over 10, 30, 30, and 35 days. It was numerically simulated using the Model Change capability in ABAQUS/Standard (Dassault Systèmes, 2023). The consolidation period of 130 days after embankment construction was simulated using the transient consolidation procedure. In the static analysis, gravity loading was activated incrementally to simulate the self-weight of the embankment fill during staged construction.

Figure 4(a) presents the settlement variation with time, comparing field-measured settlements with numerical predictions using the SANICLAY-B and MCC models for the soft clay layer. For monotonic loading cases, both SANICLAY-B and MCC provide comparable predictions and closely capture both the magnitude and rate of primary consolidation observed in the field. Figure 4(b) presents the lateral displacement profile with depth at the toe of the embankment, comparing field measurements with predictions obtained using SANICLAY-B and the built-in MCC model for the soft-clay layer.

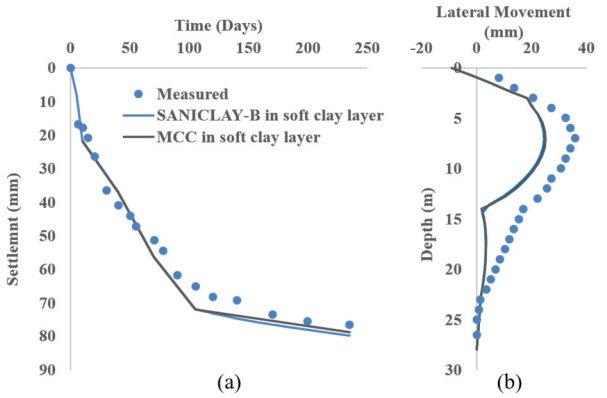


Figure 4. Comparison of simulated and predicted (a) settlements at the center (b) lateral displacement at the toe of the embankment

The measured data indicate a maximum lateral displacement of approximately 35 mm occurring at a depth of around 12–15 m, with lateral deformations reducing both above and below this depth. The numerical prediction captures the overall trend and shape of the measured profile, including the location of the maximum lateral deformation zone. However, a slight underprediction is observed between 10–20 m depth, where measured movements are slightly greater than predicted. Under monotonic loading, the SANICLAY-B and MCC formulations produce nearly indistinguishable profiles, indicating comparable performance. The close alignment between measured and predicted settlements and lateral displacements underscores the effectiveness of the implemented SANICLAY-B model in accurately capturing the time-dependent deformation behavior of soft soils during consolidation, justifying its use for cyclic loading analysis in the following sections.

## 2.3 *Cyclic Load Application*

Following successful validation of the 3D model, the embankment crest was subjected to a uniform sinusoidal surface pressure to simulate traffic-induced cyclic loading at the end of the consolidation period, assuming that the road was opened to traffic after 130 days. The applied load varied between a minimum of 5 kPa and a maximum of 30 kPa at a frequency of 1 Hz. The one-way cyclic loading was applied continuously, without rest periods, to simulate 100 cycles of closely spaced axle loads. Additional simulations were conducted at a frequency of 25 Hz and load magnitudes ranging from 5 kPa to 20 kPa, to assess the sensitivity of the soil-arching mechanism to variations in traffic loading characteristics.

# 3 RESULTS AND DISCUSSION

In light of the different cyclic responses demonstrated in Figure 3 for SANICLAY-B and MCC at element level, Figure 5 compares vertical-stress profiles with depth (measured from the embankment base) at two lateral positions (i.e., above the column at 0.75 m away from the centerline and at the mid-span subsoil at 1.2 m away from the centerline) both at the end of consolidation and after application of 100 cycles. In all cases the vertical stress above the column exceeds that in the subsoil,

confirming soil arching. The occurrence of soil arching is quantified using the stress concentration ratio ($n$), defined by Han & Gabr (2002) and given in the Table 3.

$$n = \frac{\sigma_c}{\sigma_s} \tag{13}$$

where $\sigma_c$ is the vertical stress over column and $\sigma_s$ is the vertical stress over soil in between columns at the same depth.

Table 3. Stress Concentration Ratio (SCR).

| SANICLAY-B for the soft clay | | MCC for the soft clay | |
|---|---|---|---|
| End of consolidation | End of 100 cycles | End of consolidation | End of 100 cycles |
| 1.44 | 1.39 | 1.19 | 1.14 |

From end of consolidation to 100 cycles, the profiles shift rightward over the columns (stress increase) and slightly leftward or less markedly rightward in the subsoil, indicating progressive load transfer to the stiffer inclusions. This cyclic intensification of arching is more pronounced with SANICLAY-B, which predicts higher SCR than MCC, particularly near the embankment–subsoil interface where load sharing is governed. This happens due to softening of subsoil due to cyclic degradation. The upper portion of the profiles remains comparatively similar between models, whereas differences concentrate near the embankment base. Concurrently, the modest increase in subsoil stress, reflected by a reduction in the Stress Concentration Ratio (SCR), after 100 loading cycles suggests partial degradation or redistribution of stresses under cyclic loading. Nevertheless, the dominant trend of stress concentration above the columns remains evident.

Figure 6 shows the evolution of vertical stress, with cycle number $N$ at two locations (i.e., above a column and at the mid-span subsoil) for the soft-clay layer modelled with SANICLAY-B and with the built-in MCC formulation. In all cases the column stress exceeds the subsoil stress, confirming arching. The average vertical stress (midpoint between the peak and trough of each cycle) increases gradually with $N$ for both models, with the oscillation amplitude remains nearly constant. A rapid early increase over the first 10–20 cycles is followed by a slower, asymptotic rise towards $N$=100. Relative to MCC, SANICLAY-B consistently predicts higher stresses over the columns and lower stresses in the subsoil, indicating a larger stress-concentration ratio and a more efficient redistribution of load onto the stiff inclusions throughout the loading history due to increased stiffness difference between soil and columns during cyclic degradation of subsoil. The separation between the column and subsoil curves is maintained and marginally widens with cycling, reflecting progressive arching development. Figure 7(a) illustrates the variation of vertical stress with the number of loading cycles ($N$) for both subsoil and column locations under two different loading frequencies ($f$ = 1 Hz and $f$ = 25 Hz). At the column location, the vertical stress remains higher than that at the subsoil, indicating the effectiveness of load transfer through the column. Under both frequencies, a gradual increase in mean vertical stress is observed with increasing cycles, along with superimposed fluctuations due to the cyclic nature of the applied load. Notably, the amplitude of stress oscillations is more pronounced at the higher frequency ($f$ = 25 Hz), and the stress levels at both subsoil and column locations are elevated compared to those at $f$ = 25 Hz. The results suggest that loading frequency influences the dynamic arching response within the embankment system.

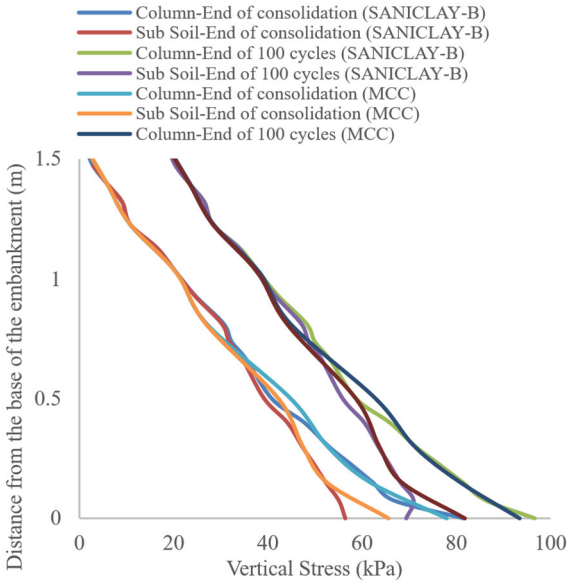


Figure 5. Evolution of vertical stress in the embankment over the column and mid-span closest to the centre at the end of consolidation and at the end of 100 cycles

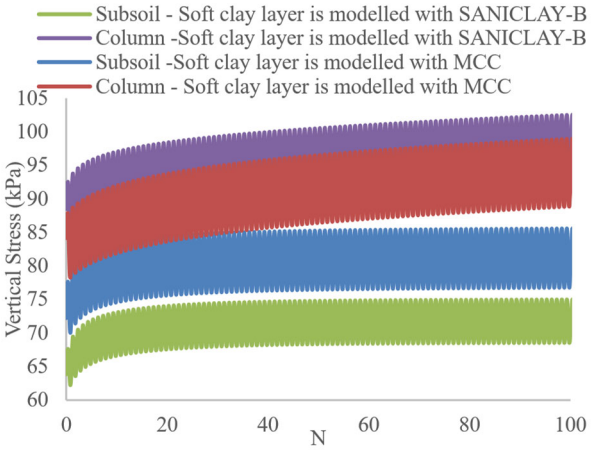


Figure 6. Evolution of vertical stress with cycle number $N$ at the column and mid-span.

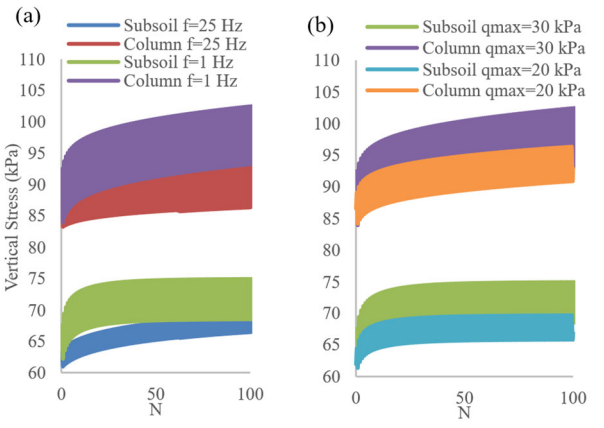


Figure 7. Effect on dynamic arching with (a) varying frequency and (b) cyclic load amplitude

Figure 7(b) illustrates the evolution of vertical stress on the column heads and in the subsoil beneath the embankment over 100 loading cycles ($N$) for two different cyclic loading amplitudes: a cyclic load with $q_{max}$=30 kPa and $q_{max}$=20 kPa. In both loading scenarios, the vertical stresses exhibit a

characteristic oscillatory pattern corresponding to the cyclic loading, superimposed on a gradually increasing mean stress. For $q_{max}$=30 kPa, the mean vertical stresses are higher, with the column experiencing greater stresses than the subsoil. In the $q_{max}$=20 kPa case, both the column and subsoil stresses are reduced, though the same trend of higher stresses in the column relative to the subsoil persists. The initial cycles show a rapid increase in mean stress, followed by a slower rate of growth as the number of cycles progresses, indicating stress redistribution.

## 4 CONCLUSIONS

This study investigated the dynamic behaviour of soil arching in column-supported embankments subjected to cyclic traffic loading, with an emphasis on the role of constitutive modelling. A three-dimensional FE model incorporating a bounding-surface plasticity model (SANICLAY-B) was developed and compared with the built-in Modified Cam Clay (MCC) formulation. The SANICLAY-B model reproduced key cyclic features observed in tests and field data with loop curvature, progressive energy dissipation, mean-strain drift, and stiffness degradation, while MCC tended to remain narrower and over-stiff during cyclic loading. Dynamic soil arching was evidenced by the progressive stress redistribution between columns and the subsoil at mid-span locations in column-supported embankments. With increasing load cycles, stresses over the columns intensified, while subsoil stresses either decreased or rose at a slower rate, demonstrating a growing concentration of stress within the columns. This trend was more consistently and markedly captured by the SANICLAY-B model. Under monotonic loading, however, both SANICLAY-B and the Modified Cam Clay (MCC) model yielded comparable predictions, indicating that the advantages of advanced plasticity models become more pronounced under cyclic loading. Parametric analyses further confirmed that the amplitude and frequency of traffic loading significantly influence the evolution of the soil arching mechanism and, consequently, the long-term stability of the system, emphasising the importance of explicitly modelling cyclic degradation in design analyses.

## 5 ACKNOWLEDGEMENTS

The authors gratefully acknowledge the International Postgraduate Scholarships awarded to the first two authors by Western Sydney University.

## 6 REFERENCES

Bi, Z., Gong, Q., Guo, P., and Cheng, Q. 2020. Experimental study of the evolution of soil arching effect under cyclic loading based on trapdoor test and particle image velocimetry. Canadian Geotechnical Journal 57(6), 903–920. https://doi.org/10.1139/cgj-2019-0205

Bian, X., Liu, S., Duan, X., Jiang, J., and Chen, Y. 2024. Dynamic soil arching effect in pile-supported embankment due to train passages at high speeds. Soil Dynamics and Earthquake Engineering 181, Article 108690. https://doi.org/10.1016/j.soildyn.2024.108690

Dassault Systèmes, 2023. ABAQUS 2023 documentation. Dassault Systèmes, Vélizy-Villacoublay, France. https://www.3ds.com/support/documentation/

Dafalias, Y.F., Manzari, M.T., and Papadimitriou, A.G. 2006. Saniclay: simple anisotropic clay plasticity model. International Journal for Numerical and Analytical Methods in Geomechanics 30(12), 1231–1257. https://doi.org/10.1002/nag.524

Han, G.-x., Gong, Q.-m., and Zhou, S.-h. 2015. Soil arching in a piled embankment under dynamic load. International Journal of Geomechanics 15(6), Article 04014094. https://doi.org/10.1061/(ASCE)GM.1943-5622.0000443

Han, J., and Gabr, M. A. 2002. Numerical analysis of geosynthetic-reinforced and pilesupported earth platforms over soft soil. Journal of Geotechnical and Geoenvironmental Engineering 128(1), 44-53.

ISO/IEC, 1991. ISO/IEC 1539-1:1991 – Information technology – Programming languages – Fortran – Part 1: Base language. International Organization for Standardization, Geneva, Switzerland

Jamsawang, P., Yoobanpot, N., Thanasisathit, N., Voottipruex, P., and Jongpradist, P. 2016. Three-dimensional numerical analysis of a DCM column-supported highway embankment. Computers and Geotechnics 72, 42–56. https://doi.org/10.1016/j.compgeo.2015.11.006

Lang, R., Ma, C., Cheng, X., Sun, L., Zhou, L., Zhang, J., Feng, S., and Li, D. 2023. Numerical analysis of dynamic behavior of piled embankment under train loading. Computers and Geotechnics 155, Article 105243. https://doi.org/10.1016/j.compgeo.2022.105243

Ma, Y., Hu, J., Xue, D., and Lü, X. 2024. Investigating soil arching in pile-supported embankments through physical experiments and DEM simulations. Geotechnical and Geological Engineering 42(5), 3857–3875. https://doi.org/10.1007/s10706-024-02762-z

Niemunis, A. 2022. Incremental driver, user's manual. University of Karlsruhe KIT, Germany.

Niu, T., Yang, Y., Ma, Q., Zou, J., and Lin, B. 2023. Dynamic soil arching in piled embankment under train load of high-speed railways. Earthquake Engineering and Engineering Vibration 22(3), 719–730. https://doi.org/10.1007/s11803-023-2195-7

Pham, H.V., and Dias, D. 2019. 3D numerical modeling of a piled embankment under cyclic loading. International Journal of Geomechanics 19(4), 315–326. https://doi.org/10.1061/(ASCE)GM.1943-5622.0001354

Roscoe, K.H., and Burland, J.B. 1970. On the generalized stress-strain behavior of "wet" clay: a review. Journal of Terramechanics, 7(2), pp. 107–108. https://doi.org/10.1016/0022-4898(70)90160-6

Seidalinov, G. 2018. Constitutive and numerical modeling of clay subjected to cyclic loading. PhD thesis. The University of British Columbia, Vancouver. Available at: https://open.library.ubc.ca/soa/cIRcle/collections/ubctheses/24/items/1.0365970 [Accessed 10th August 2025].

Seidalinov, G., and Taiebat, M. 2014. Bounding surface Saniclay plasticity model for cyclic clay behavior. International Journal for Numerical and Analytical Methods in Geomechanics 38(7), 702–724. https://doi.org/10.1002/nag.2229

Taiebat, M., Dafalias, Y.F., and Peek, R. 2010. A destructuration theory and its application to Saniclay model. International Journal for Numerical and Analytical Methods in Geomechanics 34(10), 1009–1040. https://doi.org/10.1002/nag.841

Zhou, J., Zhang, L., Zhou, S., and Deng, M. 2023. Investigation of the effect of cyclic loading on the soil arching using damped spring-based trapdoor model. Computers and Geotechnics 156, Article 105279. https://doi.org/10.1016/j.compgeo.2023.105279

Zhuang, Y., and Wang, K. 2018. Finite element analysis on the dynamic behavior of soil arching effect in piled embankment. Transportation Geotechnics 14, 8–21. https://doi.org/10.1016/j.trgeo.2017.09.001